JOURNAL OF MATERIALS SCIENCE 30 (1995) 2130–2138

Studies of diamond films/crystals synthesized by oxyacetylene combustion flame technique

W. ZHU, B. H. TAN*, J. AHN, H. S. TAN
Microelectronics Centre, School of Electrical and Electronic Engineering, Nanyang Technological University, Nanyang Avenue, Singapore 2263

High-quality diamond films/crystals were synthesized using the oxyacetylene combustion flame technique at atmospheric pressure in a narrow acetylene-rich region. Three nozzle configurations, single-, tilted- and multi-nozzle, were used to explore possible ways to improve the uniformity of diamond films and to increase the deposition areas. It was found from the systematic investigation that the surface morphology and crystal structure of diamond films are strongly dependent on the processing parameters such as the gas mixture ratio, r, of acetylene to oxygen, substrate temperature, and nozzle configurations. The appearance of two-dimensional spiral steps on (1 1 0) diamond surfaces was observed, which have not previously been reported in the literature. This phenomenon is explained using the concept of surface reconstruction. The observed layered steps on (1 0 0), (1 1 0), and (1 1 1) diamond planes strongly suggest that under certain conditions the synthetic diamond crystals could grow with a layer mechanism on any major plane, at least in the case of films made using combustion flames. Experimental results from X-ray diffraction and Raman spectroscopy show the presence of compressive stress along the ⟨1 0 0⟩ direction in the diamond films. The films also have good optical transparency, indicating potential for optical coating applications. The hardness, growth rate, film uniformity, and deposition areas of diamond films are discussed. Advantages and limitations of these three flame-torch deposition techniques are also presented.

1. Introduction

Diamond has many potential applications due to its excellent electrical, optical, mechanical, chemical and thermal properties. Its high hardness, strength, chemical resistance and low coefficient of friction makes it an ideal material for abrasive- and wear-resistant surfaces, tool coatings and corrosion barriers. The ultraviolet–visible–infrared transparency makes it suitable for optical applications, such as windows, lens coating and X-ray lithography masks. Its high thermal conductivity and good electrical insulation makes diamond film a good heat diffuser material for high-power semiconductor devices, thus allowing a high degree of circuit integration and denser packaging with fewer thermal problems. The high hole mobility, the wide band gap and the high breakdown voltage of doped diamond may lead to active semiconductor diamond elements for high-power/high-frequency electronic devices and devices to be utilized in high-temperature, chemically harsh and/or high-radiation flux environments. Diamond is estimated to have respectively, 1189 and 70 times the potential of GaAs for high-frequency/high-power and high-frequency/high-packaging density applications [1]. To realize the true potential of diamond in the above applications, diamond must be deposited as films and/or coatings on non-diamond substrates in an economically viable manner.

The development of low-pressure diamond film deposition techniques has generated a great deal of interest in the scientific community. Since the breakthrough in low-pressure synthesis of diamond, various techniques for low-pressure growth of diamond have been developed. Now diamond films can be synthesized by various chemical vapour deposition (CVD) techniques such as hot-filament CVD, microwave-assisted CVD, arc-discharge CVD, etc. The current status of extensive research activities in the growth of diamond thin films by the CVD process and in the applications of these synthetic diamond films are discussed in several excellent review articles [2–7].

The low-pressure synthesis techniques are all performed in a reduced pressure environment thus requiring a reaction chamber. The physical size of the reaction chamber poses a limitation on the size or length of the article that can be coated [8]. The low-pressure synthesis techniques usually yield low growth rates, e.g. the growth rates for the low-pressure plasma-enhanced CVD are typically 1–3 $\mu m\,h^{-1}$ [9]. Recently, Hirose first reported a new method of

* *Present address*: GINTIC Institute of Manufacturing Technology, Nanyang Technological University, Nanyang Avenue, Singapore 2263.

0022–2461

diamond synthesis using oxygen acetylene combustion flames at atmospheric pressure [10], which was later confirmed by several other groups [11–20]. Compared with conventional CVD processes, diamond growth rates of the order of 100 $\mu m\,h^{-1}$ can be realized using this method [8].

In the oxygen acetylene combustion flame technique, the high temperature of the oxyacetylene flames, about 3000 °C at its inner core near the nozzle edge [21], ionizes the hydrocarbon gas by thermal plasma, thus generating the chemical vapour species for diamond deposition. Apart from the high growth rates, this simple technique, which only requires low equipment investment, can produce high-quality diamond films/crystals with optical transparency in the visible light range, as well as in the infrared and ultraviolet ranges [22, 23]. This technique demonstrates the diversity of the methods that can be used to grow diamond. It also offers a new set of experimental possibilities to study the mechanisms of synthesis and crystal growth of diamond.

In this paper, we report experimental results from our systematic studies on diamond films/crystals synthesized using the oxyacetylene flame technique with three different nozzle configurations, and also our new observation of two-dimensional spiral steps on (1 1 0) diamond surfaces, as well as on (1 0 0) and (1 1 1) planes. This new phenomenon of growth steps on (1 1 0) surfaces is explained with the concept of surface reconstruction. Advantages and limitations of the flame diamond film deposition techniques with the three nozzle configurations, and the effects of processing parameters on the diamond films/crystals are discussed.

2. Experimental procedure

The combustion flame technique involves the burning of various hydrocarbons at atmospheric pressure. The experimental apparatus is schematically shown in Fig. 1. The oxygen–acetylene welding torch is fitted with nozzles of three different configurations, as shown in the insert of Fig. 1. In the first configuration or single-nozzle, a brazing nozzle (size no. 1), is positioned vertically above the substrate. The distance between the torch nozzle and the substrate is maintained between 8 and 14 mm, and the deposition time is 1 h. In the second tilted-nozzle configuration, the brazing nozzle (size no. 1) is tilted at an angle, ϕ, between the normal of the substrate and the flame axis. An angle of 60° has been used for most of the runs. The distance between the torch nozzle and the substrate varied between 1 and 3 mm and the deposition times were 0.5–2 h. In the third multi-nozzle configuration, a custom-made multi-nozzle is used. The distance between the torch nozzle and the substrate was between 3 and 4 mm, and the deposition time varied from 1–2 h.

The source gases used were 99.5% purity acetylene and oxygen. The flow rates of the acetylene and oxygen are controlled by mass flow controllers (MKS model 100) with an accuracy of ± 0.01 standard $l\,min^{-1}$. The oxygen gas flow rate was maintained at 1.32 standard $l\,min^{-1}$ for all the experiments, while the acetylene gas flow rates were varied in accordance to the gas ratio, r, of the acetylene to oxygen. Molybdenum substrates of 12 mm × 12 mm in size, were first polished with sandpaper, followed by 3 μm diamond paste. The polished molybdenum substrates were then cleaned in trichloroethylene, acetone and rinsed with deionized water, before being mounted on a water-cooled holder made of copper. The substrate temperature, T_S, was measured with an infrared pyrometer (Mikron model M90).

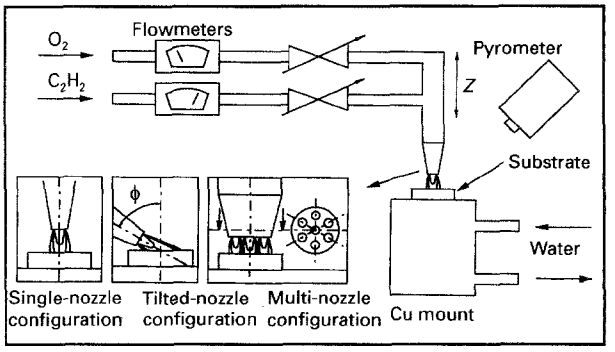

Figure 1 Schematic drawing of the oxyacetylene deposition experiment. The inserts show the single-, tilted- and multi-nozzle configurations.

The deposited diamond films were characterized using scanning electron microscopy (Joel JSM S300, Cambridge Stereoscan 250 MK3), X-ray diffractometry (Philips PW 1830), Raman spectroscopy (Spex 1403) and microhardness tests (Matsuzawa DMH-1).

3. Results and discussion

3.1. Morphology

The surface morphology and other physical properties of the flame-made diamond films are greatly affected by the deposition parameters such as gas mixture ratios of acetylene to oxygen, temperature and substrate interface, etc. For all three nozzle configurations, as the acetylene concentration in the gas mixture is increased, non-diamond phases are found to increase, gradually leading to the formation of amorphous carbon and eventually graphite and soot. This can be explained on the basis that with increasing acetylene concentration, the etching effect on graphitic components by atomic hydrogen, oxygen and OH decreases, resulting in increasing levels of non-diamond bonded phases in the films.

Diamond crystals can only be synthesized within a very narrow range of gas mixture ratio. At high gas mixture ratio, r, ball-like deposition with high amorphous carbon content was formed. But at too low a gas mixture ratio, there was no carbon deposition due to the complete oxidation. Fig. 2 shows scanning electron micrographs of the diamond film deposited using the single-nozzle configuration, with an acetylene to oxygen ratio of $r = 1.02$. The substrate temperature measured at the centre was about 980 °C. The area of deposition was about 5 mm in diameter. Fig. 2a–d show the morphology of the diamond film

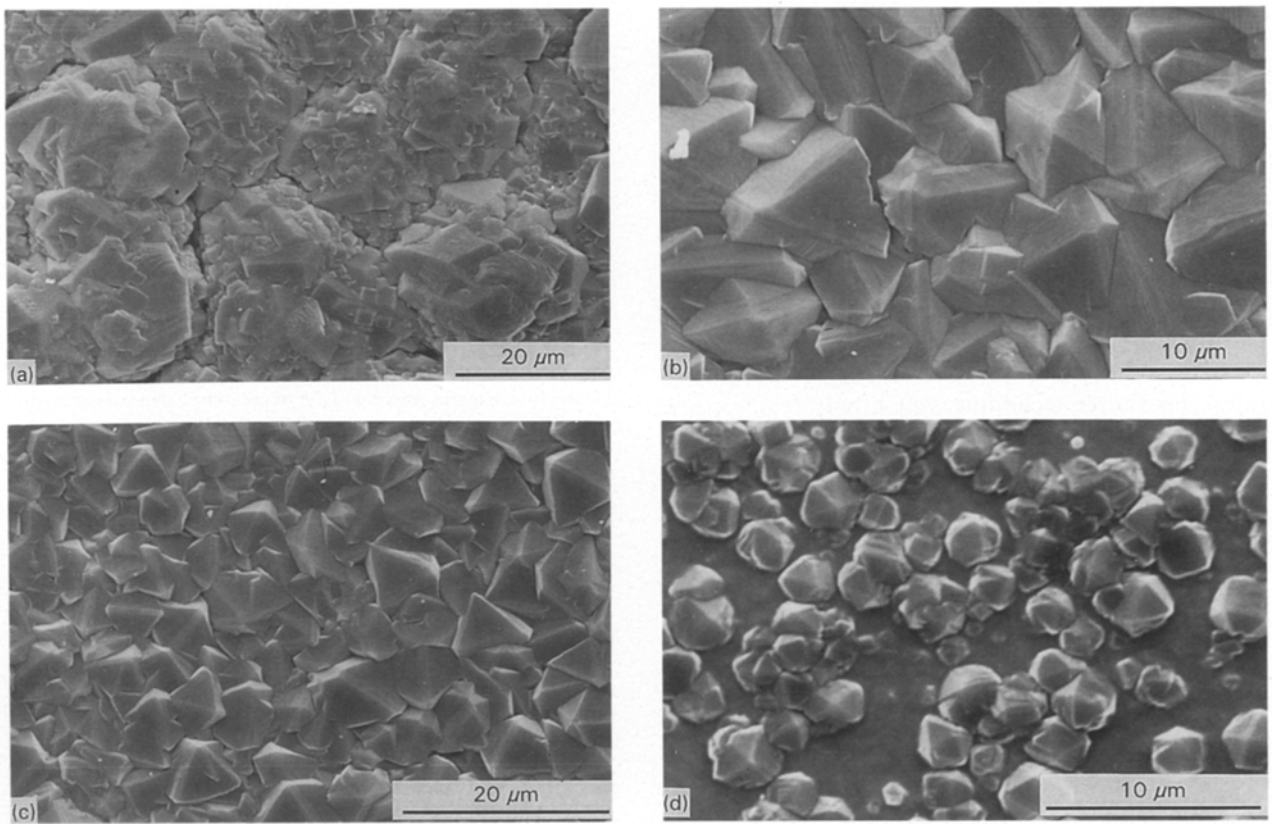

Figure 2 Scanning electron micrographs of diamond films deposited using the single-nozzle configuration with $r = 1.02$. The radial distances from the centre spot are: (a) 0 mm, (b) 1 mm, (c) 1.8 mm, (d) 2.5 mm.

at points 0, 1, 1.8 and 2.5 mm away from the film centre, respectively. The film morphology changed from Fig. 2a at the centre to Fig. 2d at the periphery of the deposit, showing the non-uniformity and surface morphology variation across the deposition area. At the centre of the deposition (Fig. 2a), diamond crystals have an average grain size of 20 μm, with a large number of small (1 0 0) oriented crystals growing on top of large crystals. It shows clearly the secondary nucleation and growth of diamond crystals. In Fig. 2b, at a region 1 mm away from the central position, crystals with sizes of 10–15 μm are observed. There is a large proportion of (1 1 0) oriented crystals in this region, indicating a decomposition of (1 0 0) crystals at a higher temperature through (1 1 0) at a middle temperature, to (1 1 1) oriented crystals at a lower temperature. The conclusion is that a cubic habit predominates at high temperatures, while octahedral faces result at low temperature [16, 24]. The densely packed diamond crystals having predominantly (1 1 1) orientation can be found at a region 1.8 mm away from the centre (Fig. 2c). At the periphery of the deposition area (Fig. 2d), scattered faceted diamond crystals of 2–4 μm in size can be observed. During the deposition process, oxygen in the surrounding air diffuses through the periphery of the flame into the inner zone. This addition of oxygen is believed to increase the atomic hydrogen concentration, resulting in the formation of high-quality diamond crystals [25]. However, the atomic hydrogen concentration in the combustion flame is quite low, estimated to be only a fraction of 10^{-4} [9, 26]. Frenklach and Wang proposed that the OH radical and atomic oxygen might also play a similar role for atomic hydrogen [27]. The accumulation of data [28] in the literature suggests that the graphite-etching capability of atomic oxygen and the OH radical can be two to three orders of magnitude greater than that of atomic hydrogen. Thus, it is believed that a higher concentration of the OH radical and atomic oxygen at the periphery of the flame contributes to the high quality of the diamond films.

We have also produced diamond films with considerable improvement in uniformity, optical transparency and relatively large deposition area, using the tilted torch deposition technique [29]. Fig. 3 shows a diamond film made by this method. In this figure, scratches and defects on the substrate can be clearly seen through the film, showing that the film is optically transparent. Fig. 4 shows two scanning electron micrographs of a diamond film synthesized with $r = 1.04$ and T_S at the film centre is about 750 °C. Fig. 4a is at the central spot, while Fig. 4b is at the edge, about 4 mm away from the centre. These two pictures are almost identical in terms of their surface morphology and vary only slightly in their particle sizes, giving evidence of the improvement in the film uniformity. It has been found in our experiments that the tilted torch deposition technique results in frequent delamination and breakage of film because of poor adhesion between the diamond films and the substrates. This is a result of the reduction in the velocity of gas flux normal to the substrate. The higher the momentum of deposition particles impacting on the substrate surface, the higher is the probability of these particles diffusing into the substrate, resulting in better

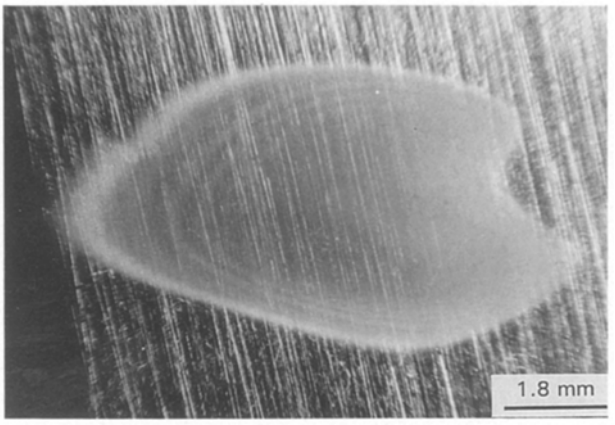

Figure 3 Optically transparent diamond film deposited using the tilted-nozzle deposition.

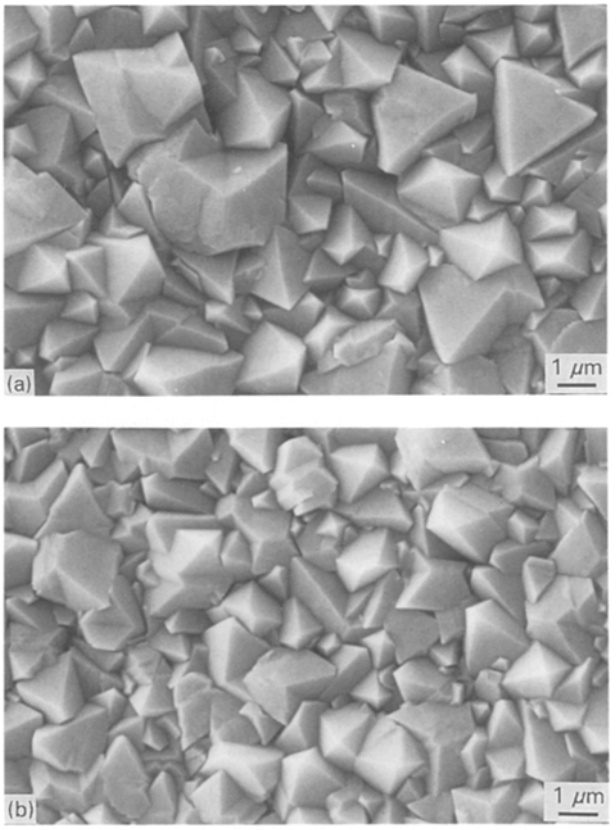

Figure 4 Scanning electron micrographs of diamond films deposited using the tilted-nozzle configuration with $r = 1.04$. They are at (a) the centre of the film and (b) the edge of the film.

adhesion. With a large tilt angle, ϕ (Fig. 1), in the tilted-nozzle configuration, a considerable amount of the gas flux momentum is parallel to the substrate surface, and does not contribute to the interface adhesion.

To increase the deposition area, we have designed and built a custom-made multi-nozzle for synthesizing diamond film. Fig. 5 shows a series of scanning electron micrographs of the surface appearance of a film deposited with an acetylene to oxygen ratio $r = 1.0$ using the multi-nozzle technique. The deposition area is about 12 mm diameter, which is three or four times larger than that produced using a single nozzle [19]. Fig. 5a–d are about 0, 3, 4 and 5 mm away from the film central spot, respectively. The substrate temperature at the deposition centre is about 875 °C. In Fig. 5a, diamond crystals with an average size of about 30 μm have the preferred (1 1 1) orientation, and this preference is extended to region (b), giving a relatively large uniform deposition area. Fig. 5c shows the appearance of (1 0 0) faces on top of triangular (1 1 1) crystals, as well as a mixture of these two oriented diamond crystals, indicating that this region is in the morphological transition field. The periphery of the deposited film is predominated by (1 0 0) faces, as shown in Fig. 5d. However, small deposition areas with no crystallographic diamond features are also observed in some samples from the multi-nozzle method. Most of these areas are scattered between the central spot and the outside regions. This may be due to the influence and/or disturbance of the gas fluxes and the distribution changes of temperature and species concentrations in the multi-nozzle flames.

The change of crystal orientation is the exact opposite to the previous observation shown in Fig. 2. These contradictory surface observations, in fact, reflect the wide debate in the literature on the diamond morphology dependence upon the processing variables. Kobashi *et al.* [30] have shown that the polycrystalline diamond films change from (1 1 1) orientation at low methane concentration, to (1 0 0) orientation as the methane concentration is increased, with a very narrow concentration range of 0.4% for causing this transformation. Spitsyn *et al.* [24] reported that high concentrations of methane in hydrogen and low substrate temperatures favoured the formation of (1 1 1) faces, while low concentrations of methane in hydrogen and high substrate temperatures produced mainly (1 0 0) faces. Within the optimum temperature range, diamond is highly faceted, but there is no consistent variation in form with temperature. With increasing temperature, changes of predominant surfaces from both (1 0 0) to (1 1 1) [31, 32] and (1 1 1) to (1 0 0) [33, 34] have been reported. From the thermodynamic equilibrium point of view, the most stable growth planes of diamond are the octahedral (1 1 1) faces, followed by (1 1 0) faces and the cube (1 0 0) faces [35]. However, the growth conditions of diamond in low-pressure CVD processes and in oxyacetylene combustion flame synthesis are far from the thermodynamic equilibrium conditions, therefore, even small shifts in processing variables, which vary from case to case, can have a significant effect on the final surface appearance. Moreover, due to the great temperature and composition gradients, high flux velocity, and high flux density in the combustion flame, non-uniformity and surface morphology variation of the flame-made diamond films/crystals are always anticipated. Therefore, caution should be exercised with interpreting the diamond surface features.

3.2. Hardness

The hardness of the synthesized films was measured by a microhardness tester (Matsuzawa DMH-1) using the Vickers indentor. It has been reported that when a measurement is performed with a light load, the

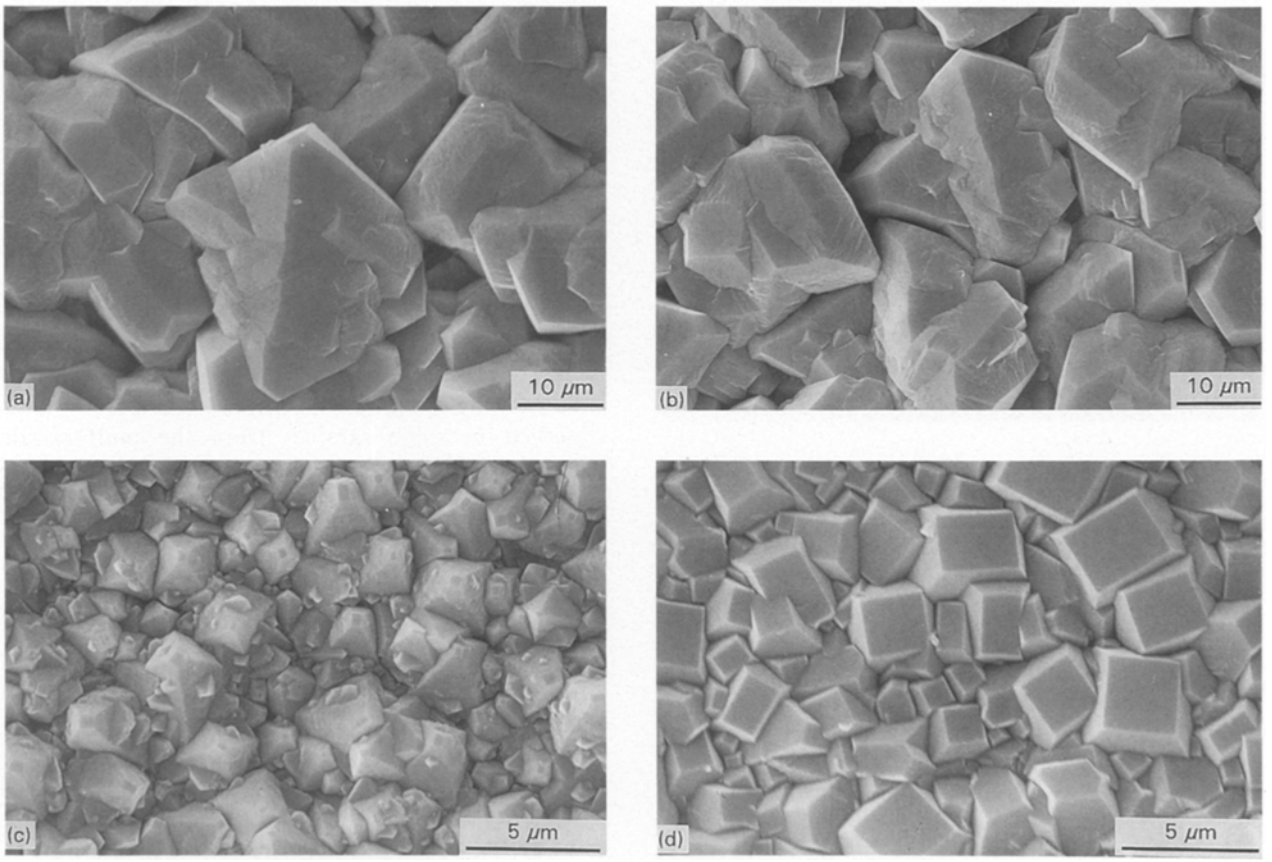

Figure 5 Scanning electron micrographs of diamond films deposited using the multi-nozzle configuration with $r = 1.00$. The radial distances from the centre sport are: (a) 0 mm, (b) 3 mm, (c) 4 mm, (d) 5 mm.

microhardness value is dependent on the load applied [36]. For measurements of thin film coating, the effect of the substrate on the film hardness measurement must be taken into account if the depth of indentation exceeds 10%–25% of the film thickness [37]. The substrate is usually thought to exert little influence when the indentation depth is less than one-tenth of the film thickness [38]. A single load of 300 g was used throughout our tests to eliminate the significance of load dependence. Table I lists the average hardness values of the different morphologies and crystal structure of the deposited diamond films. Diamond films with a ball-like structure have an average hardness of 2800 HV; while those with crystalline structure of the (1 0 0) and (1 1 1) directions have very similar average hardness values of 7800 HV and 8000 HV, respectively. Regions of the diamond film with transitional morphology between ball-like and well-defined crystalline structure have an average hardness value of 5500 HV. A maximum microhardness value of 8000 HV, obtained from the flame-made diamond films is quite close to the microhardness value of 10 000 HV for the natural diamond. From the above results, it is obvious that the hardness value is strongly dependent on the morphology and crystal structure of the diamond films.

TABLE I Average hardness value for different morphology and crystal structure of diamond films

Morphology	Hardness HV ($kg\,mm^{-2}$)
Molybdenum substrate	265
Ball-like structure	2800
Transition from ball-like to crystalline	5500
Cubic structure (1 0 0) direction	7800
Dense pinhole free (1 1 1) direction	8000

3.3. X-ray Diffraction

Fig. 6 shows two typical X-ray diffraction patterns for our diamond films. To perform the X-ray analysis, the film is peeled off the substrate and mounted on a glass sample holder. From both patterns, the diamond (1 1 1), (2 2 0), (1 1 3), (4 0 0) and (3 3 1) peaks are identified, but no graphite peak can be detected from the measurement. The results confirm that the films have mainly diamond structure. Curve (a) indicates a preference for (1 0 0) orientation in the film, because the ratios of the (1 0 0) peak to others from the film are much higher than those for the polycrystalline diamond powders (JCPDS, 6-675). For pattern (b), the ratios of the (1 1 1) peak to others from the film are much higher than those for polycrystalline diamond powders (JCPDS, 6-675), indicating the preference for the (1 1 1) orientation in the film. The peak intensity and d-spacing of the film (pattern b) and the polycrystalline diamond are listed in Table II. It is interesting to note that the d-spacing of the (4 0 0) crystal orientation of the film is smaller than that of natural diamond, whereas the others are more or less the same as those of natural diamond. This suggests the existence of compressive stress along the $\langle 1\,0\,0 \rangle$ axis in the film due to compacted lattice spacing of the planes [39].

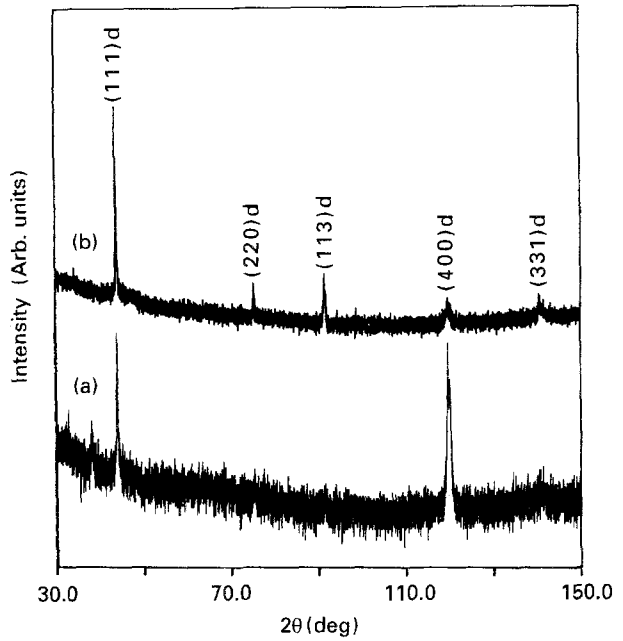

Figure 6 X-ray (CuKα) diffraction pattern of diamond films: (a) with preference for (1 1 1) orientation; (b) with preference for (1 0 0) orientation.

TABLE II X-ray data of intensity and *d*-spacing from a diamond film and from the powder diffraction of natural diamond

Index	Measured (Pattern b)		JCPDS 6-675	
	d nm	I_i/I_{max}	*d*(nm)	I_i/I_{max}
(1 1 1)	0.20602	100	0.20603	100
(2 2 0)	0.12615	7.0	0.12614	25
(1 1 3)	0.10755	9.9	0.10754	16
(4 0 0)	0.08911	4.5	0.08917	8
(3 3 1)	0.08184	1.9	0.08182	16

3.4. Raman spectroscopy

The Raman spectra at the central (1 1 1) and periphery (1 0 0) region of the film shown in Fig. 5a and b are given, respectively, in curves (a) and (b) in Fig. 7. The Raman spectrum (a) reveals a sharp diamond peak at 1332 cm^{-1}, confirming the existence of diamond crystals. The full width at half maximum (FWHM) of this spectrum is 4.5 cm^{-1}, within the top-quality range of synthetic diamond using CVD or combustion flames [6, 22, 40], although it is wider than that of natural diamond of 1.65–2 cm^{-1} [33, 41]. This curve also shows a small, broad peak around 1525 cm^{-1}, which is more pronounced in spectrum (b). The appearance of this continuous broad peak suggests the presence of sp^2 bonded carbon in the form of graphite, amorphous carbon or a combination of both. These non-diamond forms of carbon are mainly located at grain boundaries, evinced by the fact that the broad Raman peak in curve (b) is enhanced by small grains. It is plausible that this broad peak indicates the existence of various local carbon clusters with relaxed sp^2 bindings modified by surrounding vacancies [42, 43]. A striking feature of spectrum (b) is that the Raman peak excited from diamond (1 0 0) planes is located at 1338 cm^{-1}. This implies that there is a compressive

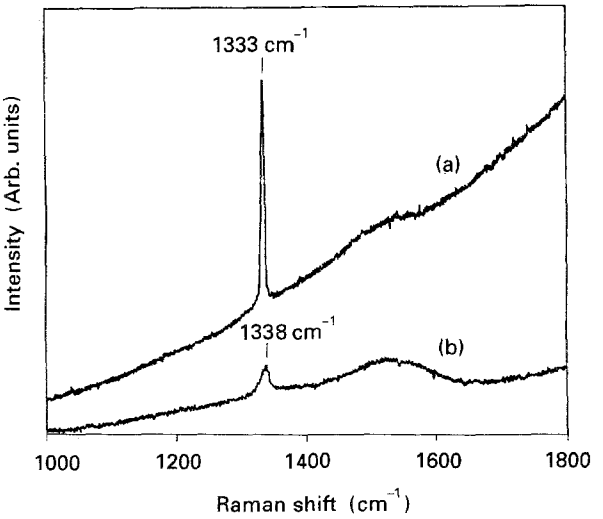

Figure 7 Raman spectra of diamond films deposited using the multi-nozzle configuration (a) at the centre with (1 1 1) surfaces, and (b) near the film edge with (1 0 0) surfaces.

stress on these (1 0 0) diamond planes [33, 44–47], which is consistent with the result found from the X-ray diffraction, as discussed in the previous section. For stress parallel to the diamond ⟨1 0 0⟩ axis, the stress can be obtained from the magnitude of the shifts by [48]

$$X = -(1.08\ \text{GPa cm}^{-1})\ \delta(k_1)$$

where $\delta(k_1)$ is the peak shift (cm^{-1}) and X is the stress (GPa). Thus the compressive stress along the ⟨1 0 0⟩ direction in the sample can be estimated to be 5.4 GPa.

3.5. Growth rate, columnar growth and interface

The combustion flame technique has the advantage of high growth rates compared to the CVD technique. Fig. 8 shows the growth rate versus the flow rate ratio, *r*, of acetylene to oxygen in the single nozzle case. The growth rate increases with the gas mixture ratio, reaching 85 μm h^{-1}. The experiments are conducted with the oxygen flow rate maintained at 1.32 standard lm^{-1}, while the acetylene flow rate is varied in accordance with the gas mixture ratio. With increase in nozzle size and flow rate, it is possible to obtain even higher growth rates of diamond films by this technique. It was also observed that the tilted nozzle deposition generally yields much lower growth rates compared with the normal flame deposition, because of the loss of a large amount of gas species flowing parallel to the substrate surface.

Fig. 9 shows a scanning electron micrograph of the rear side of the film. Diamond crystals of the order of 1 μm size can be observed from the traces of grain boundaries. Compared to the top surface of the diamond film with crystals of 30 mm size in Fig. 5, it can be deduced that during crystal growth of diamond films, the grain size increases from the substrate face to the top film surface. The protruding line shown in Fig. 9 is the replica of a scratch line on the substrate surface. Small particles can be observed on the replica

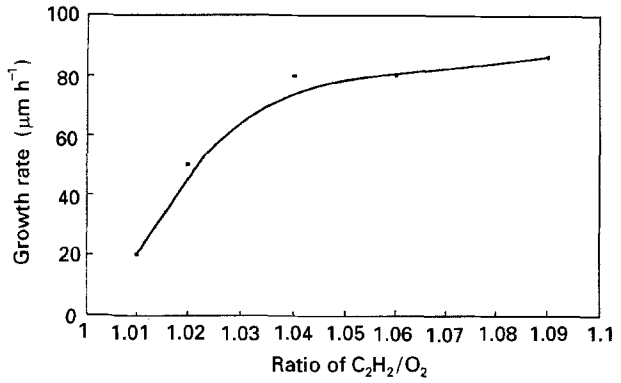

Figure 8 Growth rate of diamond films as a function of the gas mixture ratio, r, of acetylene to oxygen.

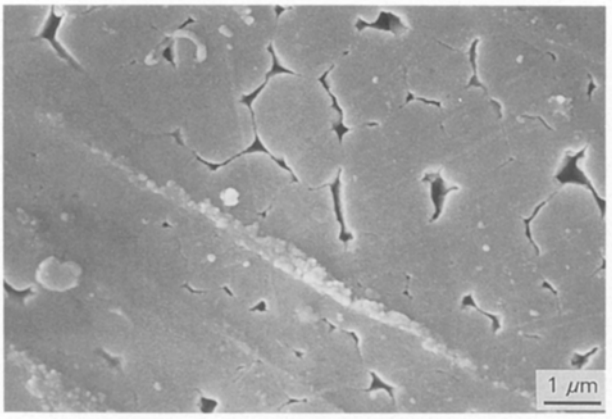

Figure 9 Scanning electron micrograph of the rearside of the diamond film.

of the scratch line, reflecting the preference for inhomogeneous nucleation at the defect regions [5, 33]. On the interface of the diamond film, which is in intimate contact with the molybdenum substrate, there are uniformly distributed small sesame-seed-like particles. These are believed to be carbides, which are formed as an intermediate layer during the deposition of diamond on molybdenum substrates and other carbide-forming substrates such as silicon, tungsten and titanium [5, 11, 49]. Fig. 10 shows a scanning electron micrograph of the columnar growth of a diamond thin film. Columnar growth is a common phenomenon in synthetic diamond films [30, 41. 50], implying that the physical properties of these diamond films are anisotropic in nature, for example, thermal conductivity.

3.6. Step-growth mechanism

An SEM micrographic observation of a film shows two-dimensional spiral steps on (1 1 0) and (1 1 1) planes in Fig. 11a and (1 0 0) planes in Fig. 11b. The layered steps indicate that the crystal growth takes place by the Burton–Cabrera–Frank mechanism [51], that is, it proceeds by a spiral growth using a screw dislocation. It is well known [52] that the glide planes in a diamond are {1 1 1} with Burgers vectors 1/2 ⟨1 0 0⟩. Therefore, the screw dislocation must be parallel to {1 1 1} planes. In fact, these two-dimensional steps can be virtually seen on any major plane in the figure. The occurrence of the layered steps strongly suggests that under certain conditions, synthetic diamond crystals can grow with the layer mechanism on any major plane, at least in the case of films made by the combustion flame technique.

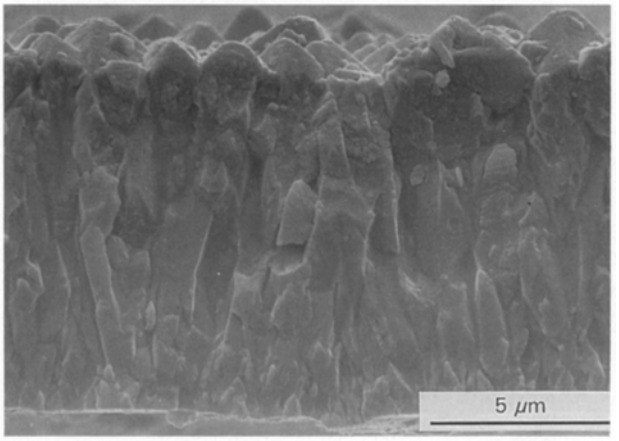

Figure 10 Scanning electron micrograph showing columnar growth of the diamond film.

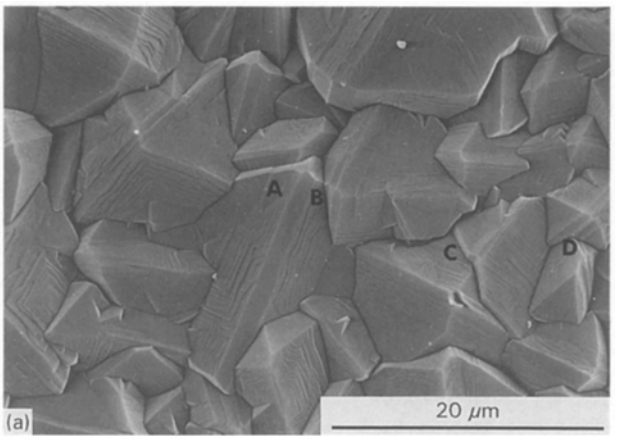

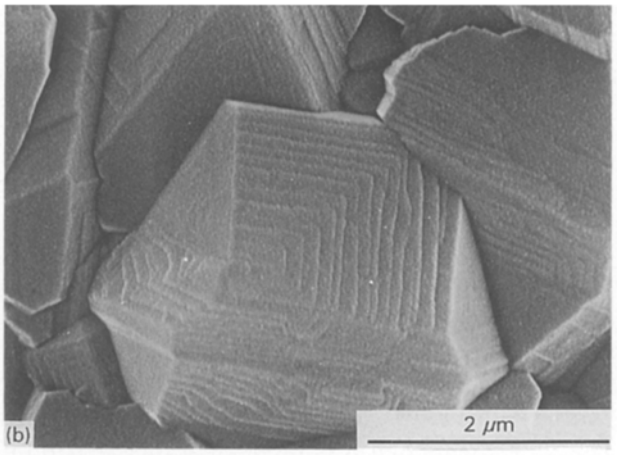

Figure 11 Scanning electron micrographs of two-dimensional steps: (a) on (1 1 0) and (1 1 1) planes; (b) on a (1 0 0) plane.

The appearance of spiral layers on (1 1 0) diamond surfaces synthesized using combustion flames is in strong contradiction with the periodic-bond-chain (PBC) theory formulated by Hartman [35]. According to the PBC theory as applied to diamonds, an uninterrupted chain of C–C bonds is called a PBC,

and diamond faces are classified into three groups, namely, flat (F), zig-zagged (S), and kinked (K), depending on the number of PBC contained in a surface layer d_{hkl}. (1 1 1) planes containing two PBC are F-planes, which have the slowest growth rate and grow by a layer mechanism; (1 0 0) planes containing no PBC are K-planes, which have the highest growth rate and should not appear as diamond facets; and (1 1 0) planes containing one PBC are zigzagged S-planes, which grow by a one-dimensional nucleation mechanism. Based on Hartman's theory, the expected diamond crystal should be an octahedron composed of (1 1 1) planes only. Apparently, our observation of two-dimensional spiral layers on (1 1 0) faces conflicts with the PBC prediction. Moreover, spiral steps on (1 0 0) planes were reported by Okada *et al.* [53], which is not consistent with the PBC theory either. The layered steps on (1 1 0) planes observed in our experiment can probably be interpreted using the concept of surface reconstruction [54]. As is known in synthetic diamond films, there is a certain number of dangling bonds on the top surface layer, thus it has high surface free energy and is in a thermodynamically unstable state. To stabilize the surface layer, surface reconstruction takes place. In such a process, an extra PBC, as well as some vacancies are created, and surface atoms rearrange in a manner to minimize the surface free energy to a crystallographically stabilized surface.

4. Conclusion

The oxyacetylene combustion flame technique has been successfully used to obtain high-quality diamond films/crystals at atmospheric pressure. The surface morphology and crystal structure depend strongly on the processing conditions, such as the gas mixture ratio of acetylene to oxygen, deposition temperature, and gas-flow conditions due to different nozzle configurations. It has been found that the microhardness of these films is closely correlated with the surface appearance and film quality. Small changes in processing variables can have a significant effect on the final surface appearance, and it is especially true in the diamond film deposition using the oxyacetylene combustion flame technique, because the deposition conditions are far from the thermodynamic equilibrium conditions. Compressive stress has also been observed along the $\langle 1\,0\,0 \rangle$ axis of the diamond crystals by both X-ray diffraction and Raman spectroscopic measurements. A relatively high growth rate is achievable with this combustion flame technique. The new observed spiral layered steps on (1 1 0) diamond planes (not previously reported in the literature) strongly suggest that under certain conditions, the synthetic diamond crystals can grow with surface reconstruction by the step-growth mechanism in any major plane, at least in the films made by the combustion flame technique.

Acknowledgements

This project has been funded by a grant from the Ministry of Finance and administered by the National Science and Technology Board, Republic of Singapore. The authors thank Mr T. H. Foo, Mr F. Tan, Mr F. H. Tan and Ms M. Y. Yong for their technical assistance.

References

1. R. ROY, *Nature* **325** (1987) 17.
2. K. E. SPEAR, *J. Am. Ceram. Soc.* **72** (1989) 171.
3. A. R. BADZIAN and R. C. DeVRIES, *Mater. Res. Bull.* **23** (1988) 385.
4. J. C. ANGUS and C. C. HAYMAN, *Science* **241** (1988) 913.
5. W. ZHU, B. R. STONER, B. E. WILLIAMS and J. T. GLASS, *Proc. IEEE* **79** (1991) 621.
6. W. A. YARBROUGH and R. MESSIER, *Science* **247** (1990) 688.
7. R. C. DeVRIES, *Ann. Rev. Mater. Sci.* **17** (1987) 161.
8. M. MURAKAWA, S. TAKEUCHI and Y. HIROSE, *Surf. Coat. Technol.* **39/40** (1989) 235.
9. M. A. CAPPELLI and P. H. PAUL, *J. Appl. Phys.* **67** (1990) 2597.
10. Y. HIROSE, "Synthesis of diamond using combustion flame in the atmosphere", Progr. and Abstracts of 1st International Conference on the New Diamond Science and Technology, Tokyo, Japan, October 1988, p. 38.
11. K. OKADA, S. KOMATSU, S. MATSUMOTO and Y. MORIYASHI, *J. Mater. Sci.* **26** (1991) 3081.
12. L. M. HANSSEN, W. A. CARRINGTON, J. E. BUTLER, and K. A. SNAIL, *Mater. Lett.* **7** (1988) 289.
13. P. G. KOSKY and D. S. McATEE, *ibid.* **8** (1989) 369.
14. W. A. YARBROUGH, M. A. STEWART and J. A. COOPER Jr, *Surf. Coat. Technol.* **39/40** (1989) 241.
15. G. JANSSEN, W. J. P. VAN ENCKEVORT, J. J. D. SCHAMINEE, W. VOLLENBERG, L. J. GILING and M. SEAL, *J. Cryst. Growth* **104** (1990) 752.
16. K. V. RAVI and A. JOSHI, *Appl. Phys. Lett.* **58** (1991) 246.
17. Y. TZENG, C. CUTSHAW, R. PHILLIPS, T. SRIVINYUNAN, A. IBRAHIM and B. H. LOO, *ibid.* **56** (1990) 134.
18. J. A. VON WINDHEIM and J. T. GLASS, *J. Mater. Res.* **7** (1992) 2144.
19. W. ZHU, B. H. TAN, J. AHN and H. S. TAN, *Diamond Rel. Mater.* in press.
20. T. ABE, M. SUEMITSU, N. MIYAMOTO and N. SATO *Appl. Phys. Lett.* **59** (1991) 911.
21. A. G. GAYDON and H. G. WOLFHARD, "Flames: Their Structure, Radiation and Temperature", 3rd Edn (Chapman and Hall, London, 1970) p. 196.
22. Y. HIROSE and S. AMANUMA, *J. Appl. Phys.* **68** (1990) 6401.
23. X. H. WANG, W. ZHU, J. VON WINDHEIM and J. T. GLASS, *J. Cryst. Growth.* in press.
24. B. V. SPITSYN, L. L. BOUILOV and B. V. DERYAGIN, *ibid.* **52** (1981) 219.
25. J. A. MUCHA, D. L. FLAMM and D. E. IBBOTSON, *J. Appl. Phys.* **65** (1989) 3448.
26. Y. MATSUI, A. YUUKI, M. SAHARA, and Y. HIROSE, *Jpn J. Appl. Phys.* **28** (1989) 1719.
27. M. FRENKLACH and H. WANG, *Phys. Rev. B* **43** (1991) 1520.
28. D. E. ROSNER and J. P. STRAKEY, *J. Phys. Chem.* **77** (1973) 690.
29. W. ZHU, B. H. TAN, Z. YIN, J. AHN and H. S. TAN, in "Evolution of Surface and Thin Film Microstructure", edited by H. A. Atwater, E. Chason, M. Grabow and M. Lagally (Materials Research Society, Pittsburgh, 1993) pp. 711–4.
30. K. KOBASHI, K. NISHIMURA, Y. KAWATE and T. HORIUCHI, *Phys. Rev. B* **38** (1988) 4067.
31. R. HAUBNER and B. LUX, *J. Refract. Hard Metals* **6** (1987) 210.
32. W. ZHU, A. R. BADZIAN and R. MESSIER, in "Diamond Optics III" edited by A. Feldman and S. Holly, (SPIE, Bellingham, Washington, 1990) pp. 187–201.

33. A. R. BADZIAN, T. BADZIAN, R. ROY, R. MESSIER and K. E. SPEAR, *Mater. Res. Bull.* **23** (1988) 531.
34. G. H. M. MA, Y. HIROSE, S. AMAMUMA, M. McCLURE, J. T. PRATER and J. T. GLASS, in "New Diamond Science and Technology", edited by R. Messier, J. T. Glass, J. E. Butler and R. Roy, (Materials Research Society, Pittsburgh, PA, 1991) pp. 587–92.
35. P. HARTMAN (Ed.), "Crystal Growth: An Introduction", (North-Holland, Amsterdam, 1973), Ch. 14, pp. 367–402.
36. H. E. BOYER (Ed.), in "Hardness Testing", edited from material compiled by the ASM Committee on Hardness Testing (ASM International, materials Park, OH, c1987) pp. 80–1.
37. G. M. PHARR and W. C. OLIVER, *MRS Bull.* **17** (7) (1992) 28.
38. N. V. NOVIKOV, M. A. VORONKIN and S. B. DUB, in "New Diamond Science and Technology", edited by R. Messier, J. T. Glass, J. E. Butler and R. Roy (Materials Research Society, Pittsburgh, PA, 1991) pp. 779–83.
39. B. D. CULLITY, "Elements of X-ray Diffraction", 2nd Edn (Addison-Wesley, Reading MA, 1978) pp. 447–78.
40. J. WAGNER, C. WILD, W. M. SEBERT and P. KOIDL, *Appl. Phys. Lett.* **61** (1992) 1284.
41. Y. SATO, C. HATA, T. ANDO and M. KAMO, in "New Diamond Science and Technology", edited by R. Messier, J. T. Glass, J. E. Butler and R. Roy (Materials Research Society, Pittsburgh, PA, 1991) pp. 537–48.
42. R. E. SHRODER, R. J. NEMANICH and J. T. GLASS, *Phys. Rev. B* **41** (1990) 3738.
43. W. ZHU, B. H. TAN, Z. YIN, J. AHN and H. S. TAN, *Diamond Rel. Mater.*, submitted.
44. M. H. GRIMSDITCH, E. ANASTASSAKIS, and M. CARDONA, *Phys. Rev. B* **18** (1978) 901.
45. D. S. KNIGHT and W. B. WHITE, *J. Mater. Res.* **4** (1989) 385.
46. L. H. ROBINS, E. N. FARABAUGH and A. FELDMAN, *ibid.* **5** (1990) 2456.
47. R. J. NEMANICH, L. BERGMAN, Y. M. LeGRICE and R. E. SHRODER, in "New Diamond Science and Technology", edited by R. Messier, J. T. Glass, J. E. Butler, and R. Roy (Materials Research Society, Pittsburgh, PA, 1991) pp. 741–52.
48. M. YOSHIKAWA, G. KATAGIRI, H. ISHIDA and ISHITANI *Appl. Phys. Lett.* **55** (1989) 2608.
49. J. AHN, F. H. TAN, H. S. TAN and W. ZHU, in "Novel Forms of Carbon", edited by C. L. Renschler, J. J. Pouch and D. M. Cox (Materials Research Society, Pittsburgh, PA, 1992) pp. 356–61.
50. H. A. HOFF, C. J. CRAIGIE, E. DANTSKER and C. S. PANDE, *Appl. Phys. Lett.* **59** (1991) 1693.
51. W. K. BURTON, N. CABRERA and F. C. FRANK, *Phil. Trans. R. Soc. Lond.* **243** (1951) 299.
52. J. P. HIRTH, "Theory of Dislocations" (McGraw-Hill, New York, 1968) pp. 353.
53. K. OKADA, S. KOMATSU, S. MATSUMOTO and Y. MORIYOSHI, *J. Cryst. Growth* **108** (1991) 416.
54. L. J. GILING and V. J. P. VAN ENCKEVORT, *Surf. Sci.* **161** (1985) 567.

Received 5 August 1993
and accepted 8 September 1994